Title
Plasma formation in holmium:YAG laser lithotripsy

Journal
Lasers in Surgery and Medicine, 55(5)

ISSN
0196-8092

Authors
Pishchalnikov, Yuri A
Behnke-Parks, William M
Stoller, Marshall L

Publication Date
2023-07-01

DOI
10.1002/lsm.23659

Peer reviewed

Accepted: 20 March 2023

DOI: 10.1002/lsm.23659

BASIC SCIENCE ARTICLE

Plasma formation in holmium:YAG laser lithotripsy

Yuri A. Pishchalnikov PhD[1] | **William M. Behnke-Parks PhD**[1] | **Marshall L. Stoller MD**[2]

[1]Applaud Medical Inc., San Francisco, California, USA

[2]Department of Urology, University of California San Francisco, San Francisco, California, USA

Correspondence

Yuri A. Pishchalnikov, PhD, Applaud Medical Inc., 953 Indiana St, San Francisco, CA 94107, USA.
Email: yuri.pishchalnikov@applaudmedical.com

Abstract

Objectives: During holmium:yttrium–aluminum–garnet (holmium:YAG) laser lithotripsy to break urinary stones, urologists frequently see flashes of light. As infrared laser pulses are invisible, what is the source of light? Here we studied the origin, characteristics, and some effects of flashes of light in laser lithotripsy.

Methods: Ultrahigh-speed video-microscopy was used to record single laser pulses at 0.2–1.0 J energy lasered with 242 μm glass-core-diameter fibers in contact with whole surgically retrieved urinary stones and hydroxyapatite (HA)-coated glass slides in air and water. Acoustic transients were measured with a hydrophone. Visible-light and infrared photodetectors resolved temporal profiles of visible-light emission and infrared-laser pulses.

Results: Temporal profiles of laser pulses showed intensity spikes of various duration and amplitude. The pulses were seen to produce dim light and bright sparks with submicrosecond risetime. The spark produced by the intensity spike at the beginning of laser pulse generated a shock wave in the surrounding liquid. The subsequent sparks were in a vapor bubble and generated no shock waves. Sparks enhanced absorption of laser radiation, indicative of plasma formation and optical breakdown. The occurrence and number of sparks varied even with the same urinary stone. Sparks were consistently observed at laser energy >0.5 J with HA-coated glass slides. The slides broke or cracked by cavitation with sparks in 63 ± 15% of pulses (1.0 J, $N = 60$). No glass-slide breakage occurred without sparks (1.0 J, $N = 500$).

Conclusion: Unappreciated in previous studies, plasma formation with free-running long-pulse holmium:YAG lasers can be an additional physical mechanism of action in laser procedures.

KEYWORDS

holmium-YAG laser, laser lithotripsy, optical breakdown, urinary calculi

INTRODUCTION

Laser lithotripsy to break urinary stones routinely uses free-running holmium:yttrium–aluminum–garnet (holmium:YAG) lasers that generate infrared laser pulses invisible to the human eye. During laser procedures, however, urologists frequently see flashes of light.[1–3] The origin and characteristics of visible light in infrared laser lithotripsy have not been understood. Is it a technical artifact, or does the infrared laser pulse generate visible light? Are there single or multiple flashes? How long do they last? When do they occur? And are they important for lithotripsy?

Cecchetti et al. reported melting of basket wires and thermocouples, accompanied by crackling noise, and asserted formation of a plasma bubble.[4] The assertion of plasma formation, however, was questioned on the following grounds.[5] First, the response time of thermocouples was argued to be insufficient to provide meaningful evidence of plasma formation, raising the question: At what point during the long laser pulse (>150 μs) would plasma formation occur? Second, plasma formation with optical breakdown is typically observed at laser intensities orders of magnitude greater than that of the holmium laser pulses. Visible light was argued to be not due to

plasma formation but rather heat-induced luminescence, black-body radiation, or artifacts of flashlamps that pump holmium crystals. Third, no acoustic transients and images of plasma formation were shown.

Here we show evidence of plasma formation using ultrahigh-speed video-microscopy,[6,7] infrared- and visible-light photodetectors, and acoustic measurements. Temporal profiles and timing of sparks are shown with urinary calcium oxalate monohydrate (COM) and cystine stones, as well as with microscope glass slides coated with synthetic hydroxyapatite (HA). Also shown are selected effects of plasma formation: enhanced absorption of laser energy, supersonic expansion of plasma products, breakage of glass slides with single laser pulse, and acoustic transients with and without sparks. These observations suggest that plasma formation can be an additional mechanism of action in laser lithotripsy.

MATERIALS AND METHODS

Laser

This study was conducted using holmium:YAG laser lithotripter (VersaPulse 100 W; Lumenis). The laser produces single laser pulses with energies ranging from 0.2 to 3.5 J/pulse, although the clinically relevant range for laser lithotripsy is typically from 0.2 to 1.0 J (Figure 1). The laser pulses can be administered at pulse repetition frequencies from 5 to 50 Hz depending on laser pulse energy (not to exceed 100 W average power). In this study, we used single laser pulses administered minutes apart.

Each laser pulse consisted of a series of intensity spikes, typical for free-running spiking-mode lasers (Figure 1). The most prominent intensity spike was usually observed at the very beginning of each laser pulse ($t = 0$ μs, Figure 1). The amplitude of this first intensity spike varied from pulse-to-pulse. Figure 1 illustrates this

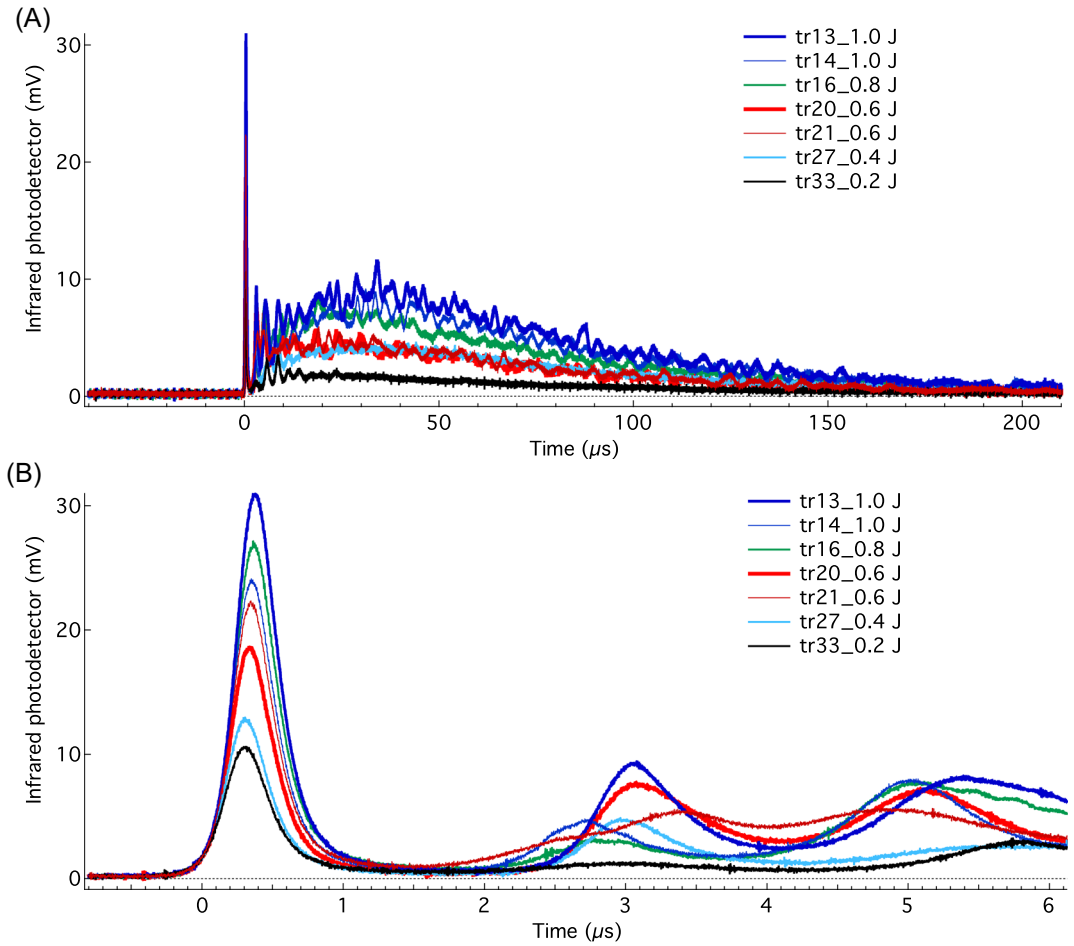

FIGURE 1 Temporal profiles of laser pulses at laser energies from 0.2 to 1.0 J measured with infrared photodetector at the output of the laser. (A) Entire pulses. (B) Enlargement showing the beginning of the laser pulses. Pulse-to-pulse variability is shown with two consecutive laser pulses at 0.6 and 1.0 J.

variability by showing two consecutive laser pulses at 0.6 J (light and heavy red traces) and at 1.0 J (light and heavy blue traces). Moreover, some laser pulses at 1.0 J could have the first intensity spike smaller than that not only at 0.8 J (green vs. light blue trace, Figure 1B) but also smaller than that at 0.6 J (not shown).

Ultrahigh-speed video microscopy

Lasering targets were positioned in a test tank with an optical port (microscope-glass slide 75 × 25 × 1 mm) at the bottom for imaging with an inverted microscope (Eclipse TS100; Nikon).[6,7] The tank was filled with degassed water either above or below the lasering target. Water absorbed infrared (2.1 μm) laser radiation blocking it from the objective of the microscope. In addition, the laser radiation was blocked by a bandpass filter (HQ535/50; Chroma Technology) mounted at the output of the microscope to reduce chromatic aberrations.

Microscope images were captured with an ultrahigh-speed camera HPV-X2 (Shimadzu). Optical magnification was achieved with a ×1 objective (Nikon Plan UW ×1/0.04, WD 3.2), a ×2.5 projection lens (Nikon CF PL×2.5), and a 19 cm extension tube (Thorlabs Inc.). The microscope was modified to increase the working distance from 3.2 to ~40 mm. The field of view was 2.25 × 3.60 mm providing a spatial resolution of 9 μm/pixel. Images were recorded at a frame rate typically from 1–5 million frames/s with an image exposure from 700 to 100 ns, respectively. No external illumination was used to record images of visible light emission during infrared laser pulses. The visible light produced by the exciter (pump) flashlamp of the laser was undetectable with the ultrahigh-speed camera settings used to collect data for this manuscript.

Infrared and visible-light photodetection

Temporal profiles and timing of infrared laser pulses and flashes of visible light were resolved with infrared and visible-light photodetectors (Thorlabs photodiodes FD05D and FDS100, respectively) with approximately 10 ns resolution. The photodetectors were positioned at about 15 cm from the distal end of the optical fiber. Selected experiments were conducted with an additional infrared photodetector (same model as the first photodetector, FD05D; Thorlabs) that served as a pick-off reference to show temporal profiles of laser pulses at the output of the laser (Figure 1). This photodetector was measuring laser pulse before the laser beam was focused into the proximal end of the optical fiber. The photodiodes were loaded with 50-Ω terminators and connected via 50-Ω coaxial cables to a 200-MHz digital oscilloscope with a 12-bit resolution (Teledyne HDO4024; LeCroy).

Triggering

The oscilloscope was triggered using either the infrared photodiode or a Rogowski coil wrapped around the high-voltage-discharge cables of the laser. Before emitting a laser pulse, the laser produced four internal pulses detected by the Rogowski coil and counted by a qualified trigger of the oscilloscope to trigger on the first laser pulse emitted in the optical fiber.

Optical fiber

The optical fiber had a cladding diameter of approximately 0.28 mm with a glass-core diameter of 242 μm (Flexiva 200; Boston Scientific).[8,9] The fiber was cleaved using high-precision optical fiber cleaver (CT08; Fujikura) to start each series of experiments with an undamaged flat fiber tip.

Lasering target

The fiber tip was positioned in contact with the lasering target, as typically done in clinical practice. We used two lasering targets: (1) whole surgically retrieved urinary stones and (2) microscope-glass slides coated with HA—the predominant form of calcium phosphate reported in 38% of urinary stones.[10] The HA-coating of the glass slide had thickness of 25 ± 5 μm (HA ~99.3%, crystallinity > 63%; Himed). An assay of how stone composition affects visible-light emission was beyond the scope of this report. Representative results are shown with a urinary COM stone and a cystine stone (Figures 2–5 and 6, respectively). The urinary COM stone contained 75% of COM, 17% of calcium oxalate dihydrate (COD), and 8% of protein. The fiber tip and the targets were positioned at the focus of the microscope using manual XYZ-translation stages with standard micrometers engraved at 25.4 μm/division (Thorlabs). Single laser pulses were applied to an intact surface of the target, repositioning it for each laser pulse.

Acoustic measurements

Acoustic transients were measured using a needle hydrophone (HNR-0500; Onda). Potential shielding by cavitation bubbles was reduced by degassing the water with a pinhole degasser.[11] The gas content was measured with a dissolved oxygen meter DO 6+ (OAKTON Instruments) and was ranging from 1 to 4 mg/L. The hydrophone was calibrated in the frequency range of 1–20 MHz and had the sensitivity ranging from 95.6 to 212 mV/MPa. The average sensitivity in the range from 1 to 5 MHz (163 mV/MPa) was used to convert hydrophone voltage to pressure. A more precise conversion would require the deconvolution with the

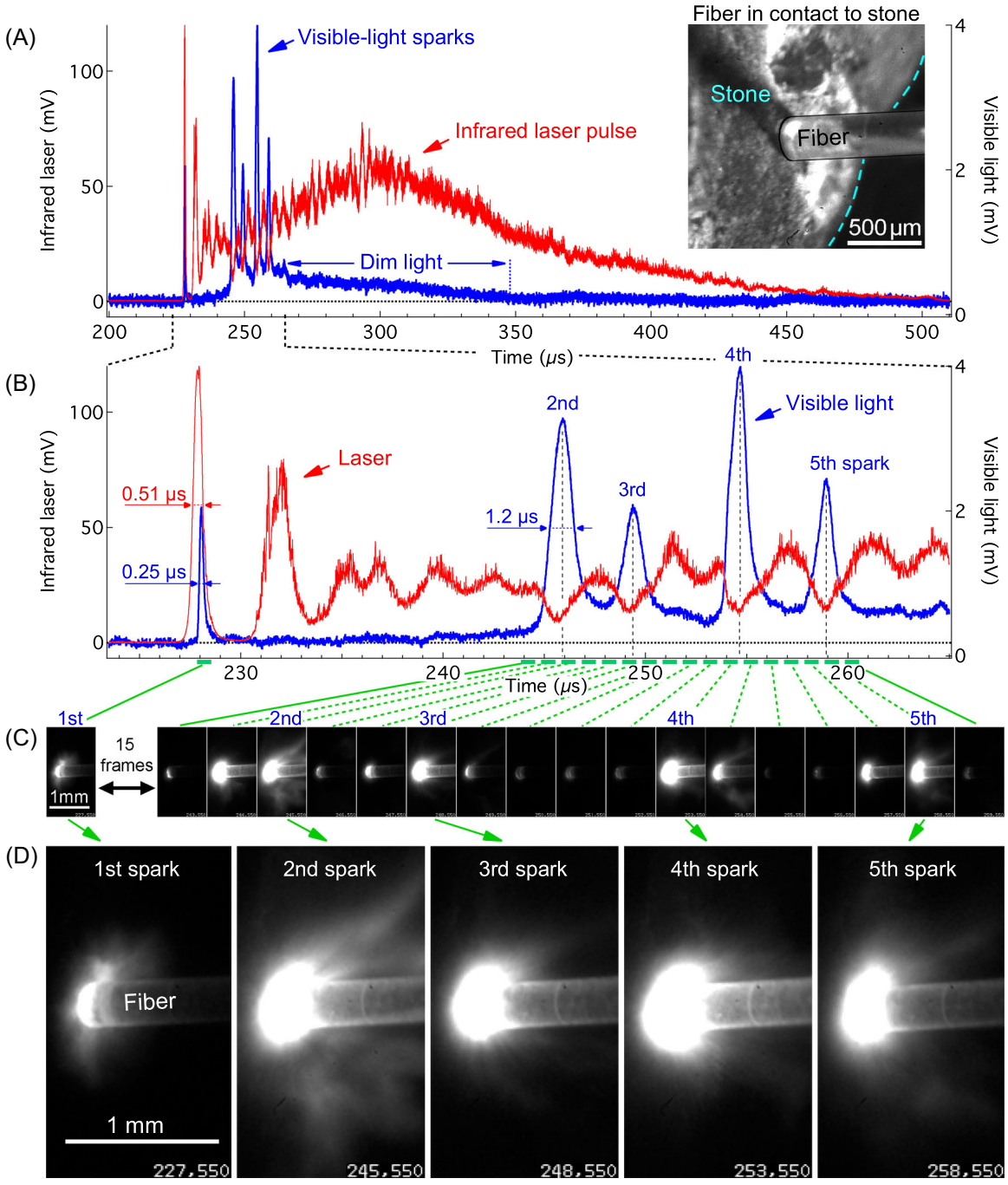

FIGURE 2 Visible-light emission with dry calcium oxalate monohydrate urinary stone in air at 1.0 J. (A) Photodiode traces showing temporal profiles of infrared laser pulse (red) and visible light (blue). (B) Enlargement of the beginning of the laser pulse (red) with five prominent sparks (blue). (C) High-speed camera sequence of images showing the dynamics of the sparks at 1 million frames/s. Timing and 700 ns exposure of the images are depicted by green lines on the time axis of photodiode traces. Fifteen frames between the first and the second sparks (black double-headed arrow) showed essentially no light and are omitted. (D) Enlarged images of the prominent sparks. The sparks were observed at the fiber tip positioned in contact with stone. The boundary of the stone is marked by a dashed cyan line on the microscope image showing the stone and glass-fiber tip before the laser pulse (top-right inset). Laser beam was coming from right to left in these images. Laser pulse consisted of many intensity spikes with various amplitude and duration, ranging from ~10 ns (limited by the photodiode resolution) to 2 µs (A, B).

impulse response, unavailable for this hydrophone. To reduce potential damage to the sensitive tip of the hydrophone, it was positioned at 10–15 mm from the fiber tip. The time of flight was subtracted to show hydrophone and photodiode traces on the same plots. Acoustic pressure is shown at distance $r = 0.3$ mm from the origin of the wave, assuming $1/r$ dependence due to the spherical divergence of waves and neglecting nonlinear absorption and supersonic velocity of shock waves. Descriptive statistics was used to calculate the means and standard deviations.

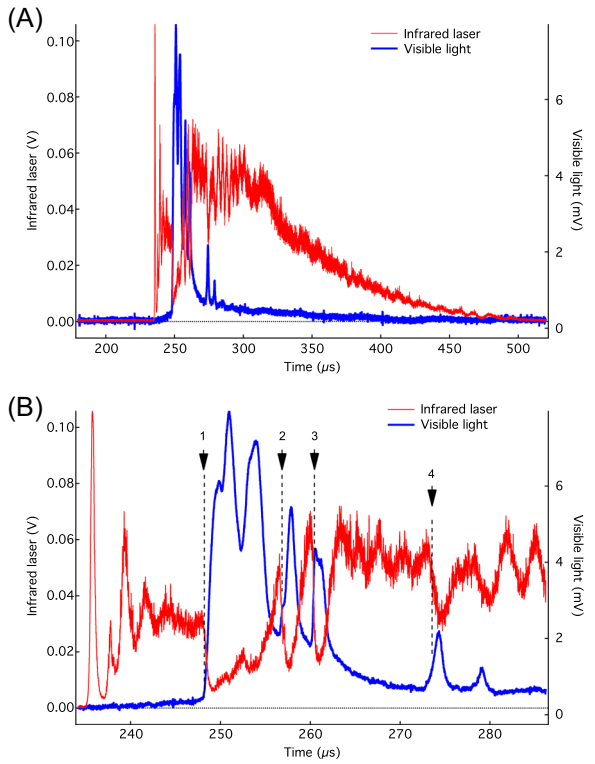

FIGURE 3 Merged sparks (dry calcium oxalate monohydrate urinary stone in air, 0.8 J). (A) Temporal profiles of infrared laser pulse (red) and visible light (blue). (B) Enlargement of the sparks. Sparks (crests, blue trace) coincided with a decrease of laser intensity detected by the infrared photodiode (troughs, red trace, arrowheads 1–4), indicating enhanced absorption of laser radiation. The first spark was ignited at 248 μs (arrowhead 1). With this laser pulse, no spark was ignited by the first intensity spike at the beginning of the laser pulse (~235 μs).

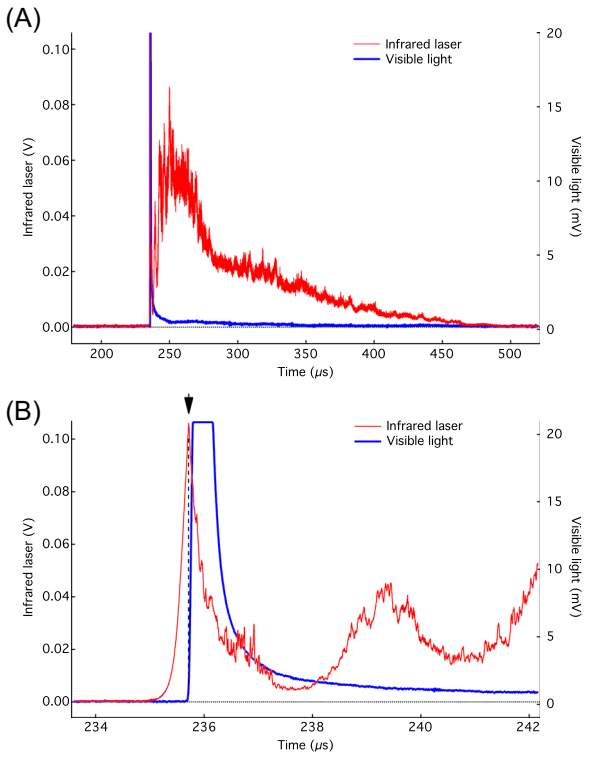

FIGURE 4 Single spark (dry calcium oxalate monohydrate urinary stone in air, 0.6 J) produced by the first intensity spike at the beginning of laser pulse. (A) Temporal profiles of infrared laser pulse (red) and visble light (blue). (B) Enlargement of the spark (clipping, blue trace). The spark enhanced absorption of laser radiation, producing an exponential decay of the infrared-photodiode trace (red) starting from the beginning of the spark (vertical dashed line) and indicating plasma formation.

RESULTS

Temporal profiles and timing of sparks

Light emission is demonstrated lasering a dry urinary stone in air at 1.0 J (Figure 2). The laser pulse started at 227 μs producing an intensity spike with the greatest amplitude (Figure 2A, infrared photodetector, red trace). The duration of this laser spike (full width at half maximum, FWHM) was 0.51 μs (Figure 2B). The spike ignited a spark (0.12-μs risetime, 0.25-μs FWHM, visible-light photodetector, blue) that ended with the first laser spike by 229 μs. The second spark was preceded with a gradually increasing dim light (<5% of peak brightness of sparks, ~239–245 μs, Figure 2B), culminated in exponentially rising bright light suggestive of optical breakdown. The second spark continued for 1.2 μs, reaching maximum at ~245.9 μs.

High-speed images (Figure 2C,D) showed that the sparks were ignited at the fiber tip in contact with the stone (microscope image of the fiber and stone before the laser pulse is shown in top-right inset of Figure 2A). The ignitions typically expanded into larger areas, expelling light-emitting products from the laser-irradiated region. Some dim light emission continued between the subsequent sparks (marked by vertical dashed lines in Figure 2B), fading away approximately 90 μs after the sparks (Figure 2A, 260–350 μs).

Light emission between sparks could vary from undetectable (as between the first and second sparks, Figure 2) to almost as bright as the sparks—making it difficult to distinguish individual sparks (Figure 3). These merged sparks could last for tens of microseconds (Figure 3). In contrast, solitary sparks typically lasted for a fraction of a microsecond (Figure 4). Dim light after the spark could either fade away or evolve into another spark (Figure 5).

Variability of light emission with urinary stones

The occurrence, timing, and number of sparks varied even with the same urinary stone (Figures 2–5). This stone (75% COM, 17% COD, and 8% protein) showed light in 96% of pulses (65% sparks and 31% dim light without sparks, 1.0 J, $N = 20$). Another stone (41%

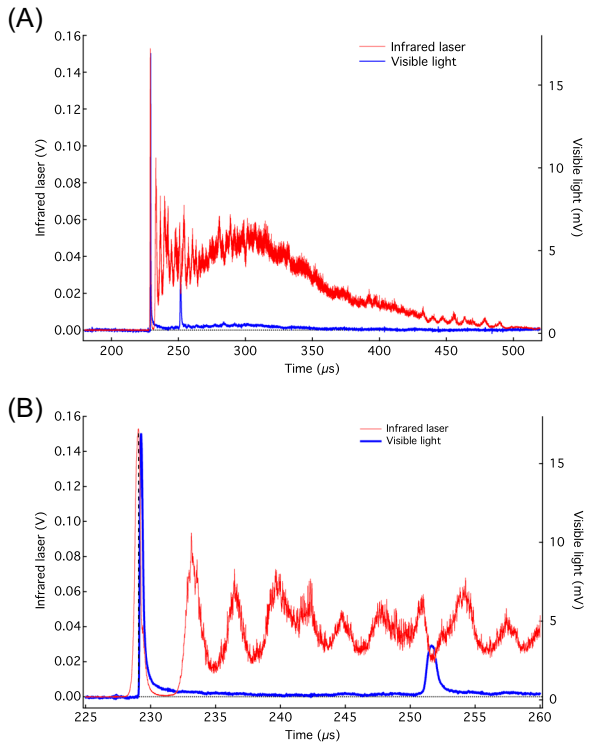

FIGURE 5 Two sparks interconnected by dim light (dry calcium oxalate monohydrate urinary stone in air, 1.0 J). (A) Temporal profiles of infrared laser pulse (red) and visible light (blue). (B) Enlargement of the beginning of the laser pulse with sparks. The laser pulse (red) started at 228.23 μs producing the first intensity spike with duration of 1.2 μs and maximum at 229 μs. The spike ignited the first spark (blue) with maximum at 229.27 μs and duration of 0.29 μs (full width at half maximum, spark duration at 10% of peak amplitude was 0.8 μs). The second spark was ignited at ~252 μs and was connected with the first spark by dim light. The dim light continued for ~150 μs. Total duration of the laser pulse was ~265 μs.

COM, 45% COD, and 14% protein) showed light in 100% of pulses (60% sparks and 40% dim light without sparks, 1.0 J, $N = 20$). Three trials with another stone (76% COM, 14% COD, 10% uric acid) showed light in 100% of pulses with 67%, 100%, and 89% of sparks during first 6–9 pulses until apparent fiber-tip damage. Damaged fibers produced mostly dim light (93%) with occasional (7%) sparks ($N = 13$). Lasering a cystine stone produced sparks in 67% of laser pulses (1.0 J, $N = 30$). Uric acid was the only composition tested that did not produce flashes of light (1.0 J, $N = 10$).

Enhanced absorption of laser radiation

Sparks (peaks, blue traces) were seen to coincide with troughs in infrared-photodiode traces (red), indicative of enhanced absorption of laser radiation (Figures 2–4). The enhanced absorption was observed with both solitary sparks (e.g., Figure 4) and merged sparks (Figure 3), starting from the beginning of the first spark (dashed line, Figure 4). The absorption of laser radiation is further demonstrated using two infrared photodetectors showing laser pulse at the pick-off reference at the output of the laser before the optical fiber (photodetector 1) and infrared radiation scattered from the stone (photodetector 2, Figure 6). Photodetector 2 showed an enhanced absorption of laser radiation starting from the initiation of sparks (vertical dashed lines at 0.1 and 2.7 μs, Figure 6B). The enhanced absorption of laser radiation was indicative of plasma formation.

Supersonic expansion of light-emitting products

High-speed camera images showed that the light-emitting products expanded supersonically pluming from the irradiated region (Figure 7). The supersonic expansion of sparks generated cracking sound in air and shock waves in water.

HA-coated glass slides (HA-slides) in water

Generation of shock waves is demonstrated lasering HA-slides in water. Figure 8 shows the temporal profile of the laser pulse measured with a pick-off reference photodetector, visible-light emission, and acoustic pressure. Flashes of light (blue) were associated with the intensity spikes in the temporal profile of the laser pulse (black), producing the most intense spark at the very beginning of the laser pulse. Only this first spark generated a shock wave (dark red), whereas the subsequent sparks produced no shock waves.

No shock waves were observed from the second spark even when it had similar risetime, duration, and amplitude as that of the first spark (Figure 9B, 236.5 μs). Likewise, no shock waves were observed from the subsequent sparks (Figure 9B). High-speed images showed that the first spark was surrounded by liquid, whereas the subsequent sparks were in a vapor bubble (Figures 8B and 9C,D).

Cavitation bubbles were formed at both the proximal and distal surfaces of the slide. The bubbles collapsed (706 and 951 μs, Figure 9A) and rebound (1.2 and 1.3 ms, Figure 9A) generating shock waves hundreds of microseconds after the end of the laser pulse. Peak pressure from the collapsing bubbles reached 60 MPa (Figure 9A, inset, 951 μs).

Acoustic transients with and without sparks

Greatest peak pressure from sparks was 58 ± 5 MPa (mean ± SD, $N = 5$, 0.6 J). Such shock waves (Figure 10A) were generated by the first spark produced with the flat fiber tip in contact with the flat surface of

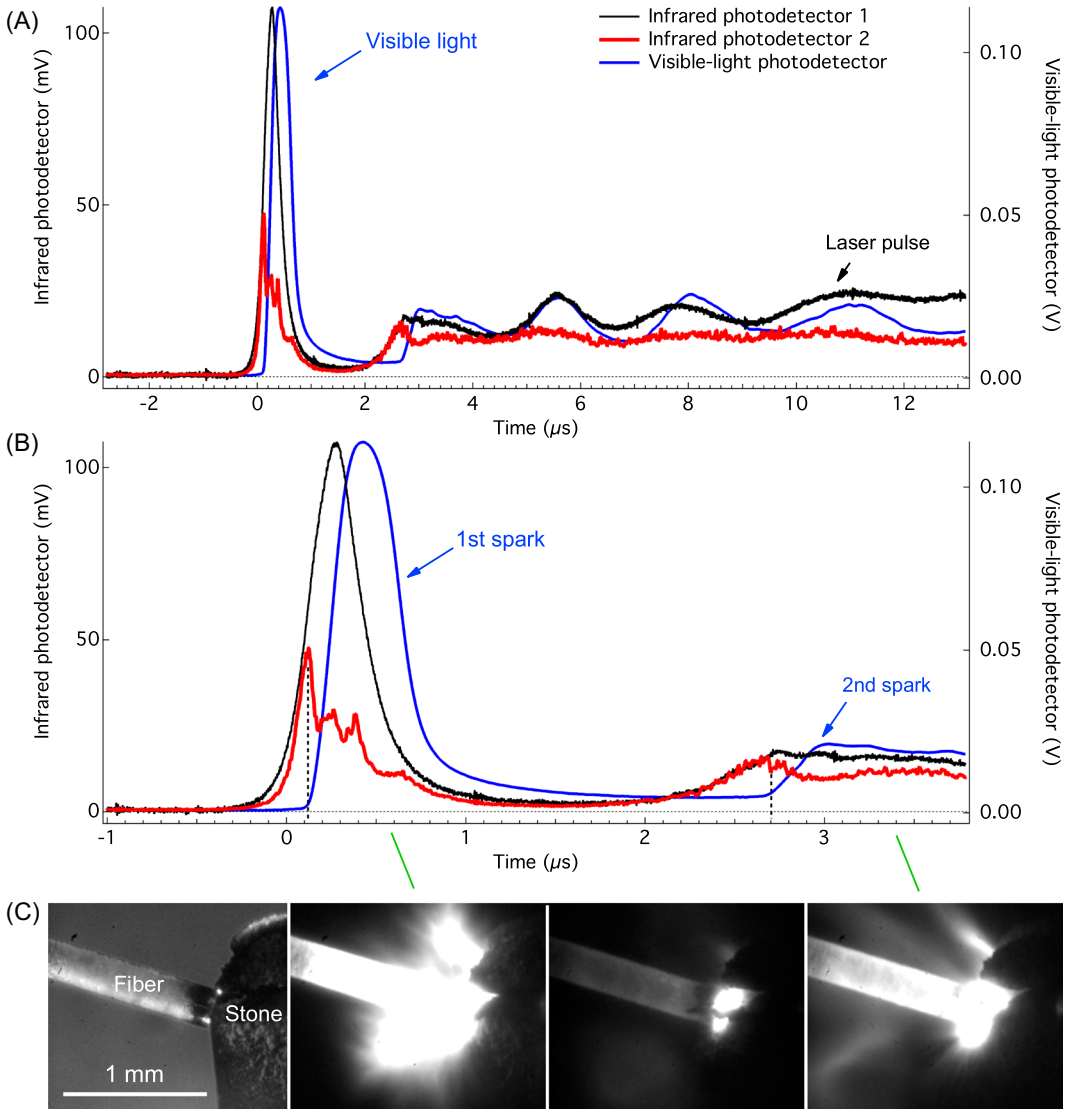

FIGURE 6 Sparks at the surface of a cystine stone during a laser pulse at 1.0 J in air. (A) Traces recorded with visible-light (blue) and infrared (black and red) photodetectors. (B) Time enlargement of the first intensity spike at the beginning of the laser pulse. Infrared radiation was measured with two photodetectors: photodetector 1 (black trace) measured the laser pulse at the pick-off reference at the output of the laser before the optical fiber, while photodetector 2 (red trace) measured infrared radiation scattered from the stone. Photodetector 2 showed a reduction of the signal in comparison with that of photodetector 1, starting from the initiation of sparks (vertical dashed lines at 0.1 and 2.7 μs, B). (C) High-speed camera images recorded with a 2 μs step between frames and showing the first two sparks. Left frame shows a microscope image of the fiber in contact with the stone surface before the laser pulse. Laser beam was coming from left to right in these images.

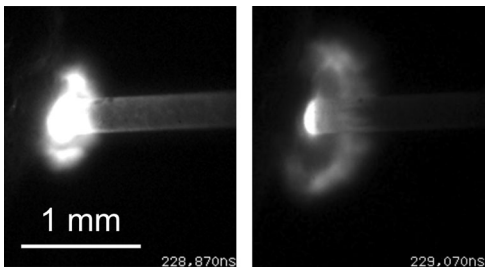

FIGURE 7 High-speed camera images of the first spark in Figure 5. Images were recorded at 5 million frames/s with an exposure of 100 ns. During the 200 ns interval between frames, light-emitting products expanded at 0.31 ± 0.06 mm, traveling supersonically with a speed of 1.5 ± 0.3 mm/μs and producing cracking sound in air.

HA-slides in water. Subsequent sparks were in expanding bubbles and generated no shock waves (Figure 10A, inset). Shock waves from the collapsing bubbles produced peak pressure of 51 ± 18 MPa ($N = 5$, 0.6 J).

An increase of laser energy to 1.0 J did not show an increase of peak pressure (48.4 ± 8.4 MPa from sparks and 59.2 ± 22.4 MPa from bubbles, three trials with 20 pulses: $N = 3 \times 20$). A decrease of laser energy to 0.5 J made the first spark intermittent. Without the first spark, pressure waves generated at the beginning of laser pulse had amplitude ~50 times smaller than that with the first spark and had no shock front (Figure 10B). The subsequent light emission in a bubble generated no shock waves (inset, 265–315 μs).

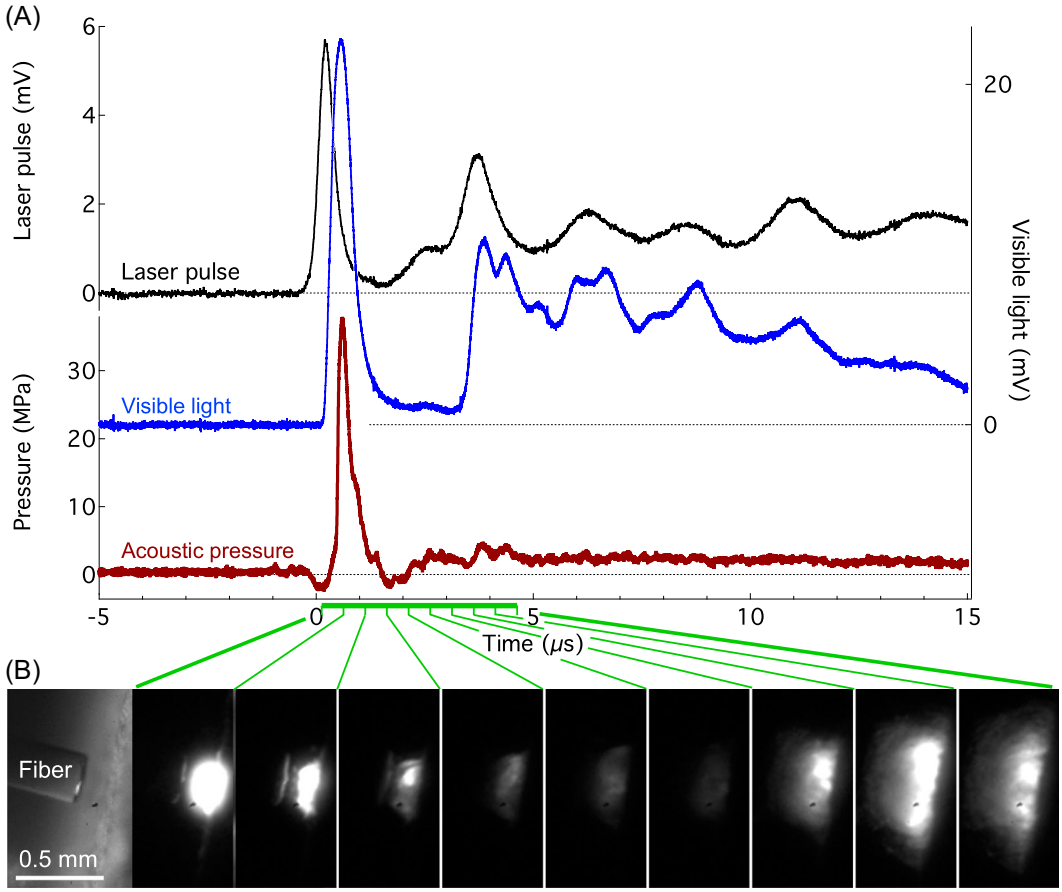

FIGURE 8 Sparks and shock waves produced by a laser pulse at 0.6 J in water at the surface of hydroxyapatite (HA)-slide. (A) Traces recorded with the infrared photodetector at the pick-off reference at the output of the laser (black), the visible-light photodetector (blue), and the hydrophone (dark red). (B) High-speed camera images recorded at 2 Mfps and showing the dynamics of the first two sparks. The first frame shows a microscope image recorded before the laser pulse and showing the fiber tip positioned at a standoff distance of 0.13 mm from the surface of the HA-slide. Laser beam was coming from left to right in these images. The beginning and end of the high-speed camera frames is depicted on the time axis by green lines. The first spark was surrounded by liquid and produced a shock wave. The subsequent sparks were in a vapor bubble and produced no shock waves. Hydrophone trace (dark red) was shifted forward to offset the travel time of acoustic wave from the fiber tip to the hydrophone.

No light was observed lasering uncoated glass slides in water (Figure 10C). Similarly, no light was observed lasering water with no target (Figure 10D). Without sparks, peak pressure (produced during the laser pulse) was one to two orders of magnitude smaller than that with the spark (Figure 10).

Sparks with cavitation could break HA-slides in water by a single laser pulse (Figure 11). No slides were broken by cavitation without sparks (water, 1.0 J, $N = 500$) and by sparks without cavitation (air, 1.0 J, $N = 3 \times 20$). In contrast, sparks with cavitation broke or cracked HA-slides in $63 \pm 15\%$ of laser pulses (1.0 J, $N = 3 \times 20$).

DISCUSSION

This study shows evidence of plasma formation with a conventional free-running holmium laser. Temporal profiles of laser pulses showed many intensity spikes of various duration and amplitude (Figures 1–5) typical for free-running lasers.[12–14] The intensity spike at the beginning of laser pulse could produce a spark that generated a shock wave in the surrounding liquid, whereas the subsequent sparks in a vapor bubble generated no shock waves in the liquid (Figure 9). This is because the liquid-confined plasma expansion during the first spark could build up pressure pushing against almost incompressible liquid, whereas plasma expansion during the subsequent sparks was essentially unconfined pushing against compressible gas in the expanding bubble. Another factor was the mismatch of acoustic impedances (~10^4) at the gas–water interface transmitting through the bubble wall only a fraction of the acoustic energy (~0.1%).

Water absorbs holmium:YAG laser energy decreasing it exponentially with the distance by ~63% at 0.3–0.4 mm.[14,15] In addition, the divergence of laser beams decreases laser intensity with the distance from the fiber tip.[3] Therefore, the smaller the distance, the greater

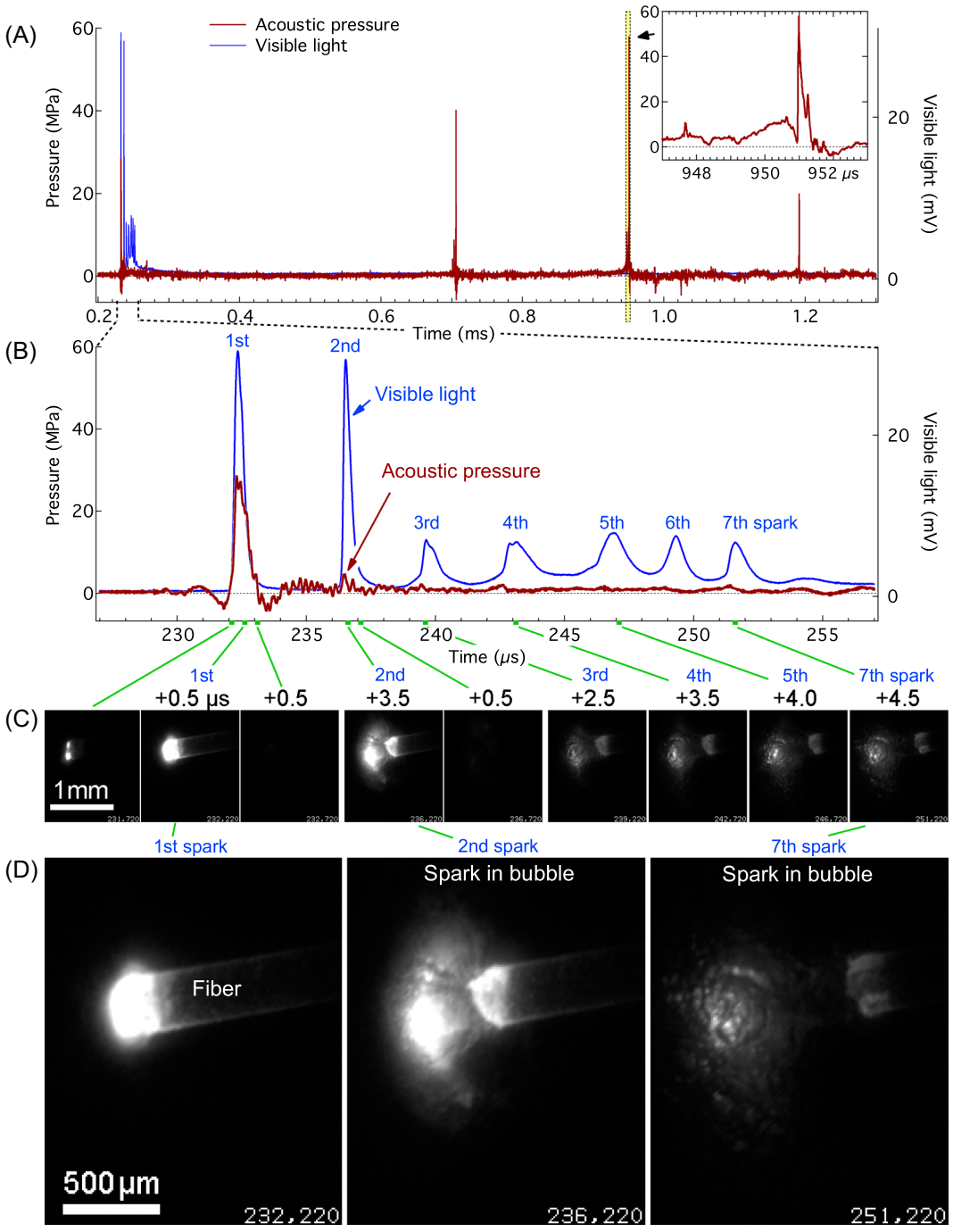

FIGURE 9 Sparks and shock waves in water produced by a laser pulse at 0.8 J. This laser pulse broke the hydroxyapatite-coated glass slide as shown in Figure 11. (A) Traces recorded with the visible-light photodetector (blue) and the hydrophone (dark red). Top-right inset shows an enlargement of the strongest shock wave from the collapsing bubbles. (B) Enlargement of the initial portion of traces showing all seven sparks produced by this laser pulse. (C) High-speed camera images showing the dynamics of the sparks. Timing and 200 ns exposure of images are depicted on the time axis by green lines and bars. (D) Enlarged images of the first (left), second (center), and seventh (right) sparks. The first spark was surrounded by liquid, whereas the subsequent sparks were in a vapor bubble. The first spark produced a shock wave, whereas the subsequent sparks produced no shock waves. Hydrophone trace (dark red) was shifted forward by 8.97 μs, offsetting the travel time of acoustic waves from the fiber tip to the hydrophone (13.4 ± 0.1 mm).

the laser intensity at the target and the likelihood of optical breakdown.

Optical breakdown is a stochastic process that occurs when laser radiation ionizes target material above some critical value (>10^{18} electrons/cm^3).[15] Initially, free electrons can be released by thermionic emission and, accelerated by the electromagnetic field, ionize other atoms, releasing more electrons. The avalanching proliferation of free electrons can lead to optical breakdown provided that laser intensity overcomes quenching losses

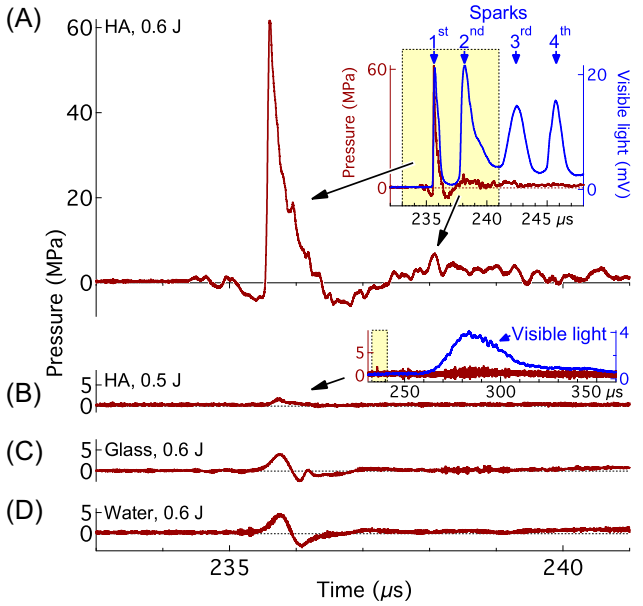

FIGURE 10 Acoustic pressure in water with (A) and without (B–D) sparks at the beginning of laser pulse. (A) Shock wave generated by a spark at the surface of hydroxyapatite (HA)-coated slide at 0.6 J. Top-right inset shows the first four sparks (blue trace) at the beginning of the pulse (dotted-line rectangle highlights the time span of the main plot). The first spark (inset, ~236 μs) was ignited before the expansion of a vapor bubble (high-speed camera images are not shown) and generated the shock wave (dark red). Subsequent sparks were in a bubble (images not shown) and produced no shock waves. (B) Without a spark at the beginning of laser pulse (HA-slide, 0.5 J, inset, dotted-line rectangle), the pressure wave had amplitude of ~2 MPa and no shock front. The visible-light photodetector showed no substantial light emission until the dim light later during the laser pulse (inset, blue, 270–310 μs). (C) Hydrophone signal recorded at laser energy of 0.6 J lasering glass slide without HA coating and with no light emission observed. (D) Hydrophone signal recorded at 0.6 J with no target in water. No light emission was observed. Without sparks, the peak pressure of acoustic transients was one order of magnitude smaller than that with sparks.

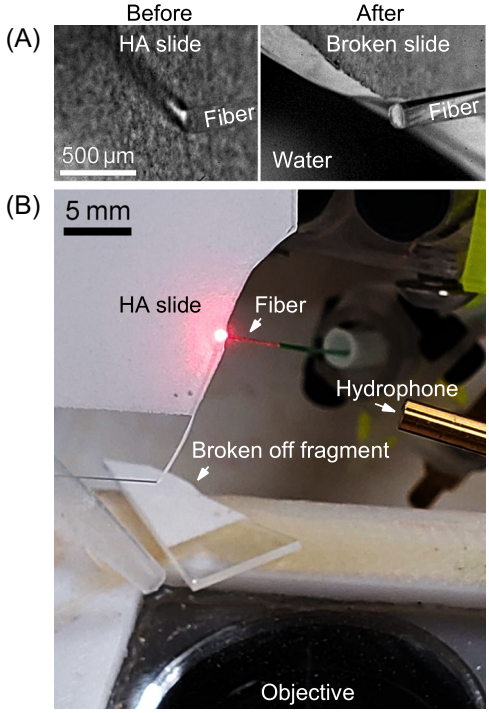

FIGURE 11 Hydroxyapatite (HA)-coated glass slide broken with a single laser pulse at 0.8 J in water. Light emission and shock waves produced during this laser pulse are shown in Figure 9. (A) Microscope images of the slide before (left) and after (right) the laser pulse. Before the pulse, the fiber tip was in contact with the slide (a faintly visible shadow was cast on the slide). After the pulse, the fiber is distinctly visible over the broken edge of the slide. (B) Photograph of the experimental setup showing the HA-slide broken by the laser pulse. An auxiliary red laser was used for aiming and was turned on for visualization of the fiber tip in this image.

(mainly inelastic collisions and diffusion of free electrons from irradiated regions).[15]

Unique and important feature of plasma formation is an increase of absorption of laser radiation.[15] Ionization generates an electrically conductive plasma that readily absorbs electromagnetic radiation creating hot spots in otherwise not so absorptive regions. Without absorption of laser energy, lithotripsy is impossible. Conversely, plasma formation along the light path to the stone can shield the transmission of laser radiation to the stone.[15]

Holmium:YAG laser lithotripsy was reported to be due to laser-induced heating and vaporization of stone constituents and interstitial water.[15–20] Plasma formation enhances absorption of laser radiation promoting heating, melting, vaporization, chemical decomposition, and microexplosions at the stone surface (not shown).

The role of cavitation has recently been reassessed suggesting that the collapsing bubbles contribute to stone breakage.[13] We observed that plasma formation can intensify cavitation effects to the level when sparks and shock waves (Figure 9) break glass slides with a single laser pulse (Figure 11).

Light emission varied even with the same urinary stone (Figures 2–5). In general, light emission depended on stone-surface geometry, fiber-to-stone distance, fiber-tip degradation, laser energy, and stone mineral composition—ranging from frequent sparks with COM stones to no light emission with uric acid stones (1.0 J, $N = 10$). Further studies are needed to assess the extent of plasma formation with urinary stones of various composition.

The flashes of light might be a mix of plasma formation and chemical decomposition or combustion of stone constituents. Previous studies with a pulsed dye laser have shown that the spectral profile of the flash accompanying the ablation of calculi differs with time delay: spectra obtained early in the laser pulse consist of an intense continuum with superimposed absorption lines, whereas spectra obtained at a longer delay show that the continuum has weakened, and calcium emission lines have appeared.[21,22] The present results suggest a need for follow-up studies to assess plasma generation using light-emission spectroscopy with a submicrosecond time-gate resolution.

This study has limitations due to its in vitro design and homogeneity of synthetic targets. Most urinary stones are heterogeneous,[23] and there is no perfect stone model for the present investigation.[24,25] The surface flatness of the synthetic targets was another idealization allowing us to position the fiber tip in close contact with the HA-slides. Observations with the HA-coated glass slides were biased toward cavitation because bubbles were formed on both the proximal and distal surfaces of the slide. Another caveat of using HA as a model material to infer laser interactions with urinary stones is that stones of various chemical composition (COM, COD, uric acid, cystine, etc.) may have different optical properties.

Here we used the conventional gold-standard holmium:YAG laser lithotripter. Similar studies might be relevant to the new thulium-fiber laser that also was observed to produce light emission with sparks, correlated with stone ablation rates.[26]

CONCLUSION

Conventional free-running holmium:YAG infrared lasers can produce flashes of visible light with relatively dim light and bright sparks. Sparks were seen to enhance absorption of laser radiation, indicative of plasma formation and optical breakdown. Sparks could produce shock waves in water at the beginning of laser pulse. These observations suggest that plasma formation can be an additional mechanism of action in laser lithotripsy and potentially in other procedures.

ACKNOWLEDGMENTS

Research reported in this publication was supported by the National Institute of Diabetes and Digestive and Kidney Diseases of the National Institutes of Health under Award Number R43DK129104. The content is solely the responsibility of the authors and does not necessarily represent the official views of the National Institutes of Health.

CONFLICT OF INTEREST STATEMENT

The authors declare no conflict of interest.

ORCID

Yuri A. Pishchalnikov http://orcid.org/0000-0003-0277-3544

REFERENCES

1. Schafer SA, Durville FM, Jassemnejad B, Bartels KE, Powell RC. Mechanisms of biliary stone fragmentation using the Ho:YAG laser. IEEE Trans Biomed Eng. 1994;41(3):276–83. https://doi.org/10.1109/10.284946
2. Dushinski JW, Lingeman JE. High-speed photographic evaluation of holmium laser. J Endourol. 1998;12(2):177–81. https://doi.org/10.1089/end.1998.12.177
3. Vassar GJ, Teichman JMH, Glickman RD. Holmium:YAG lithotripsy efficiency varies with energy density. J Urol. 1998;160(2):471–6. https://doi.org/10.1016/S0022-5347(01)62927-6
4. Cecchetti W, Zattoni F, Nigro F, Tasca A. Plasma bubble formation induced by holmium laser: an in vitro study. Urology. 2004;63(3):586–90. https://doi.org/10.1016/j.urology.2003.09.010
5. Teichman JMH, Glickman RD, Chan KF, Jansen ED, Welch AJ. Plasma bubble formation induced by holmium laser. Urology. 2005;65(3):627–8. https://doi.org/10.1016/j.urology.2004.04.082
6. Pishchalnikov YA, Behnke-Parks WM, Schmidmayer K, Maeda K, Colonius T, Kenny TW, et al. High-speed video microscopy and numerical modeling of bubble dynamics near a surface of urinary stone. J Acoust Soc Am. 2019;146(1):516–31. https://doi.org/10.1121/1.5116693
7. Pishchalnikov YA, Behnke-Parks W, Maeda K, Colonius T, Mellema M, Hopcroft M, et al. Experimental observations and numerical modeling of lipid-shell microbubbles with calcium-adhering moieties for minimally-invasive treatment of urinary stones. Proc Meet Acoust. 2019;35(1):020008. https://doi.org/10.1121/2.0000958
8. Kronenberg P, Traxer O. Lithotripsy performance of specially designed laser fiber tips. J Urol. 2016;195(5):1606–12. https://doi.org/10.1016/j.juro.2015.10.135
9. Knudsen BE. Laser fibers for holmium:YAG lithotripsy: what is important and what is new. Urol Clin North Am. 2019;46(2):185–91. https://doi.org/10.1016/j.ucl.2018.12.004
10. Herring LC. Observations on the analysis of ten thousand urinary calculi. J Urol. 1962;88(4):545–62. https://doi.org/10.1016/S0022-5347(17)64842-0
11. Kaiser AR, Cain CA, Hwang EY, Fowlkes JB, Jeffers RJ. A cost effective degassing system for use in ultrasonic measurements: the multiple pinhole degassing system. J Acoust Soc Am. 1996;99(6):3857–9. https://doi.org/10.1121/1.415211
12. Levin BA, Aldoukhi AH, Black KM, Hall TL, Roberts WW, Ghani KR. Burnback: the role of pulse duration and energy on fiber-tip degradation during high-power laser lithotripsy. Lasers Med Sci. 2021;36(9):1817–22. https://doi.org/10.1007/s10103-020-03199-5
13. Ho DS, Scialabba D, Terry RS, Ma X, Chen J, Sankin GN, et al. The role of cavitation in energy delivery and stone damage during laser lithotripsy. J Endourol. 2021;35(6):860–70. https://doi.org/10.1089/end.2020.0349
14. Frenz M, Pratisto H, Konz F, Jansen ED, Welch AJ, Weber HP. Comparison of the effects of absorption coefficient and pulse duration of 2.12-μm and 2.79-μm radiation on laser ablation of tissue. IEEE J Quantum Electron. 1996;32(12):2025–36. https://doi.org/10.1109/3.544746
15. Niemz MH. Laser-tissue interactions. 4th ed. Berlin, Germany: Springer International Publishing; 2019. https://doi.org/10.1007/978-3-030-11917-1
16. Beghuin D, Delacretaz GP, Schmidlin FR, Rink K. In: Delacretaz GP, Godlewski G, Pini R, Steiner RW, Svaasand LO, editors. Fragmentation process during Ho:YAG laser lithotripsy revealed by time-resolved imaging. *Proc. SPIE 3195, Laser-Tissue Interaction, Tissue Optics, and Laser Welding III*. Bellingham, Washington USA: SPIE; 1998. p. 220–4. https://doi.org/10.1117/12.297905
17. Chan KF, Vassar GJ, Pfefer TJ, Teichman JMH, Glickman RD, Weintraub ST, et al. Holmium:YAG laser lithotripsy: a dominant photothermal ablative mechanism with chemical decomposition of urinary calculi. Lasers Surg Med. 1999;25(1):22–37. https://doi.org/10.1002/(SICI)1096-9101(1999)25:1<22::AID-LSM4>3.0.CO;2-6
18. Shalini S, Frank DS, Aldoukhi AH, Majdalany SE, Roberts WW, Ghani KR, et al. Assessing the role of light absorption in laser lithotripsy by isotopic substitution of kidney stone materials. ACS Biomater Sci Eng. 2020;6(9):5274–80. https://doi.org/10.1021/acsbiomaterials.0c00790

19. Taratkin M, Laukhtina E, Singla N, Tarasov A, Alekseeva T, Enikeev M, et al. How lasers ablate stones: in vitro study of laser lithotripsy (Ho:YAG and Tm-fiber lasers) in different environments. J Endourol. 2021;35(6):931–6. https://doi.org/10.1089/end.2019.0441
20. Zhong P, Tong HL, Cocks FH, Pearle MS, Preminger GM. Transient cavitation and acoustic emission produced by different laser lithotripters. J Endourol. 1998;12(4):371–8. https://doi.org/10.1089/end.1998.12.371
21. Teng P, Nishioka NS, Anderson RR, Deutsch TF. Optical studies of pulsed-laser fragmentation of biliary calculi. Appl Phys B Photophys Laser Chem. 1987;42(2):73–8. https://doi.org/10.1007/BF00694813
22. Teng P, Nishioka NS, Anderson RR, Deutsch TF. Mechanisms of laser-induced stone ablation. Proc. SPIE 0712, Lasers in Medicine. Bellingham, Washington USA: SPIE; 1987. p. 161–5. https://doi.org/10.1117/12.937334
23. Sherer BA, Chen L, Yang F, Ramaswamy K, Killilea DW, Hsi RS, et al. Heterogeneity in calcium nephrolithiasis: a materials perspective. J Mater Res. 2017;32(13):2497–2509. https://doi.org/10.1557/jmr.2017.153
24. Frank DS, Aldoukhi AH, Roberts WW, Ghani KR, Matzger AJ. Polymer-mineral composites mimic human kidney stones in laser lithotripsy experiments. ACS Biomater Sci Eng. 2019;5:4970–5. https://doi.org/10.1021/acsbiomaterials.9b01130
25. King JB, Katta N, Teichman JMH, Tunnell JW, Milner TE. Mechanisms of pulse modulated holmium:YAG lithotripsy. J Endourol. 2021;35(S3):S29–36. https://doi.org/10.1089/END.2021.0742
26. Hutchens TC, Blackmon RL, Irby PB, Fried NM. Hollow steel tips for reducing distal fiber burn-back during thulium fiber laser lithotripsy. J Biomed Opt. 2013;18(7):078001. https://doi.org/10.1117/1.JBO.18.7.078001

How to cite this article: Pishchalnikov YA, Behnke-Parks WM, Stoller ML. Plasma formation in holmium:YAG laser lithotripsy. Lasers Surg Med. 2023;55:503–514. https://doi.org/10.1002/lsm.23659